Materials Transactions, Vol. 46, No. 10 (2005) pp. 2295 to 2297

RAPID PUBLICATION

Surface Evolution during Focused Ion Beam Micro-Machining in (001) Plane of Single-Crystalline Ni and Amorphous Nickel Alloy

Hiroyuki Hosokawa[1], Takeshi Nakajima[1], Koji Shimojima[1] and Mamoru Mabuchi[2]

[1]*Materials Research Institute for Sustainable Development, National Institute of Advanced Industrial Science and Technology (AIST), Nagoya 463-8560, Japan*
[2]*Department of Energy Science and Technology, Kyoto University, Kyoto 606-8501, Japan*

A focused Ga^+ ion beam (30 keV and 187 pA) have been irradiated at doses of 8.92×10^{16}–2.68×10^{18} ions/cm^2 in (001) plane of a single-crystalline Ni and an amorphous $Ni_{75}B_{15}Si_{10}$ alloy and their surface evolution was investigated by atomic force microscopy. The root-mean-square (rms) roughness increased with increasing ion dose and the transition of surface morphology from dot structure to ripple structure occurred during FIB machining in the single-crystalline Ni. However, the amorphous $Ni_{75}B_{15}Si_{10}$ alloy showed no such transition of surface morphology and held the rms roughness almost constant in an ion dose range more than about 1×10^{17} ions/cm^2. Therefore, it is suggested that surface diffusion, which is the primary smoothing mechanism for crystalline surfaces, plays an important role in smoothening during FIB machining when the ion dose is low, while viscous flow, which is dominant for amorphous surfaces, contributes to smoothening when the ion dose is large.

(Received August 2, 2005; Accepted September 12, 2005; Published October 15, 2005)

Keywords: *single-crystal, amorphous, focused ion beam, surface morphology*

1. Introduction

Development of high-performance micro-devices and micro-machines leads to further progress of information, biological, medical, and environmental technologies. Hence, it is required to establish advanced nano- and micro-machining techniques. Machining using a focused-ion-beam (FIB) is one of promising nano- and micro-machining techniques.[1–4] FIB process can machine most materials due to sputtering phenomenon. However, because ion sputtering phenomenon results from an ion-solid interaction,[5] the presence of grain boundaries, internal defects, other phases different from the matrix phase and differences in crystal orientation of each grain cause surface roughening during FIB machining.[6,7] Therefore, single-crystalline or amorphous materials are expected to be clean-cut machined, comparing to polycrystalline materials containing grain boundaries, etc. Actually, the surface of a single-crystalline Si by FIB machining was made smoother:[6,8] a die with high precision was made of single-crystalline Si by FIB machining.[8] Also, amorphous materials were clean-cut machined by FIB.[9] However, surface properties may evolve differently each other because the smoothing mechanism in a single-crystalline surface is different from that in an amorphous surface. Therefore, in this study, a single-crystalline Ni(001) and an amorphous $Ni_{75}B_{15}Si_{10}$ alloy are machined by FIB and their sputtered surfaces are investigated by atomic force microscope (AFM).

2. Experimental Procedures

A single-crystalline Ni and an amorphous $Ni_{75}B_{15}Si_{10}$ alloy were used. The single-crystalline Ni was obtained from Nilaco Corporation. The $Ni_{75}B_{15}Si_{10}$ alloy was quenched into ribbon shape using a single roller melt-spinner equipment under Ar atmosphere. A copper wheel was used at a velocity of 2500 rpm and the liquid was ejected at an overpressure of 0.06 MPa. Ribbon was obtained with an average thickness of 20 μm and width of 5 mm. Hexagon holes with 5 μm sides were machined using a FIB device, SMI2050 (Seiko Instruments Inc.). FIB machining was performed by scanning a 30 keV Ga^+ ion beam, with a nominal spot size of 35 nm and a current of 187 pA, from side to side and up and down with a 43% beam overlap and a 200 μs pixel dwell time. The fabrication time was 60–1800 s. The incident angle of the ions was set at 0 degrees. The Ga^+ ions were irradiated in (001) plane for single-crystalline Ni. The ion dose was 8.92×10^{16}–2.68×10^{18} ions/cm^2. The microstructure for an amorphous $Ni_{75}B_{15}Si_{10}$ alloy was investigated by transmission electron microscope (TEM). The surface after FIB machining was observed by scanning electron microscope (SEM). The surface roughness of the machined samples was measured by AFM, SPA300/SPI3800N (Seiko Instruments Inc., Japan).

3. Results and Discussion

TEM photograph of a $Ni_{75}B_{15}Si_{10}$ sample is shown in Fig. 1. From the electron diffraction pattern, a hallo pattern was observed, confirming that the $Ni_{75}B_{15}Si_{10}$ sample is amorphous.

SEM micrographs of hexagon holes with the side of 5 μm by FIB machining at a dose of 8.92×10^{17} ions/cm^2 for the single-crystalline Ni and the amorphous $Ni_{75}B_{15}Si_{10}$ alloy are shown in Fig. 2. The depth of holes was approximately 0.5 μm. The surfaces of walls and bottoms were very flat and smooth for both the single-crystalline Ni and the amorphous $Ni_{75}B_{15}Si_{10}$ alloy, compared to a polycrystalline.[6]

Evolution of surface morphology during FIB machining for the single-crystalline Ni is shown in Fig. 3, where the ion dose is (a) 8.92×10^{16} ions/cm^2 and (b) 8.92×10^{17} ions/cm^2, respectively. Dot structure was formed by FIB machining at the dose of 8.92×10^{16} ions/cm^2, as shown in Fig. 3(a). At the dose of 8.92×10^{17} ions/cm^2, however,

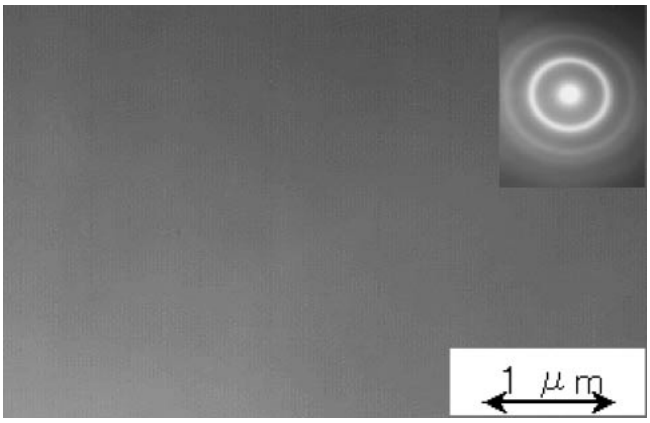

Fig. 1 TEM image of the $Ni_{75}B_{15}Si_{10}$ solid with the inset showing the electron diffraction pattern.

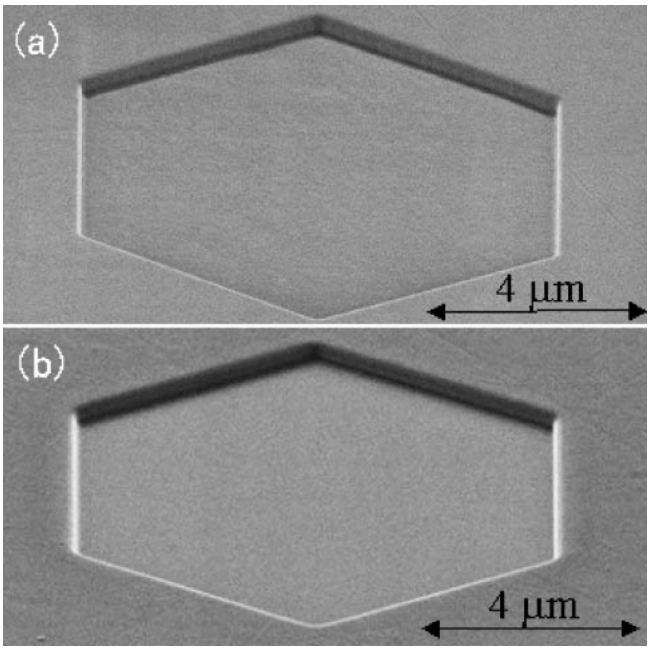

Fig. 2 SEM micrographs of hexagon holes with the side of 5 μm on (a) the single-crystalline Ni and (b) the amorphous $Ni_{75}B_{15}Si_{10}$ alloy after FIB machining at the ion dose of 8.92×10^{17} ions/cm^2.

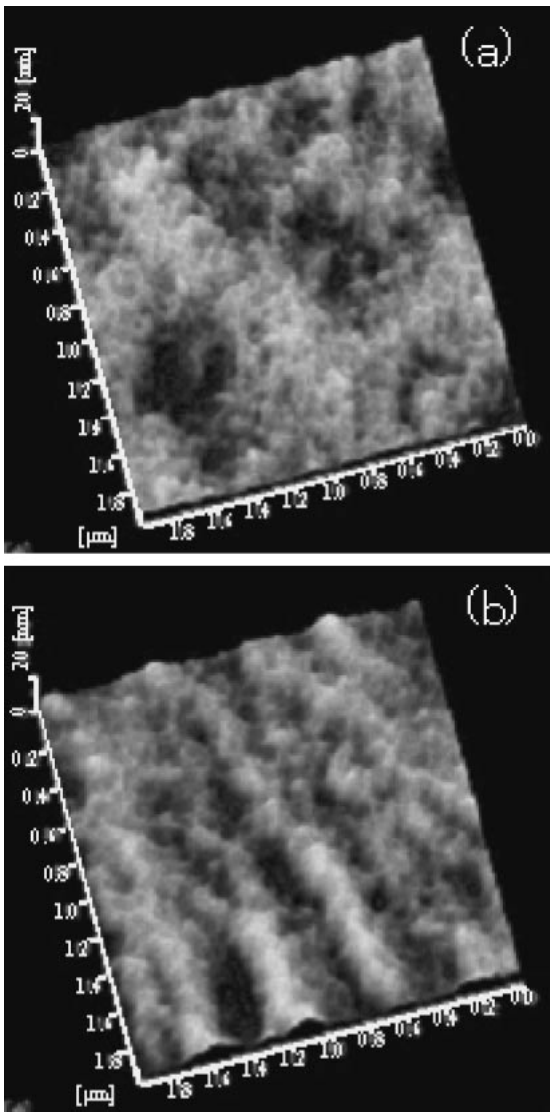

Fig. 3 3D AFM images of the surface topography of hexagon holes on the single-crystalline Ni after the bombardment of 30 keV Ga^+ ion at 0°. The ion dose is (a) 8.92×10^{16} ions/cm^2 and (b) 8.92×10^{17} ions/cm^2, respectively.

ripple structure was conspicuous. Thus, the transition of surface morphology from dot structure to ripple structure occurred during FIB machining in the single-crystalline Ni. However, the surface structure at the dose of 8.92×10^{16} ions/cm^2 was almost the same as that at the dose of 8.92×10^{17} ions/cm^2 and the transition of surface morphology was not found in the amorphous $Ni_{75}B_{15}Si_{10}$ alloy. It should be noted that evolution of surface morphology in the amorphous solid was different from that in the single-crystalline solid.

The variation in root-mean-square (rms) roughness as a function of ion dose for the single-crystalline Ni and the amorphous $Ni_{75}B_{15}Si_{10}$ alloy is shown in Fig. 4. The rms roughness significantly increased in an initial stage up to an ion dose of 8.92×10^{16}–1.78×10^{17} ions/cm^2; however, subsequently, it hardly increased with increasing ion dose for the amorphous $Ni_{75}B_{15}Si_{10}$ alloy. On the other hand, for

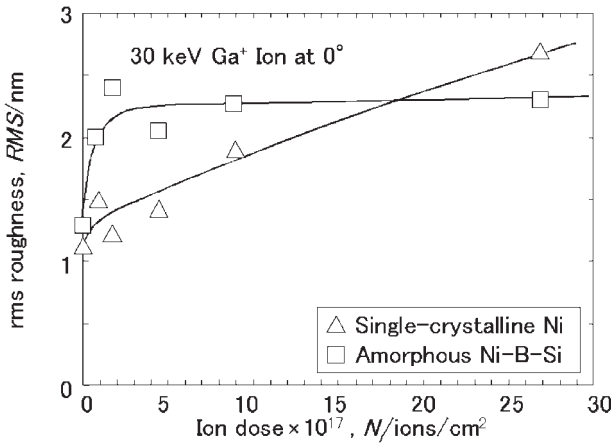

Fig. 4 Variation in root-mean-square (rms) roughness as a function of ion fluence for the bottoms of the hexagon holes on the single-crystalline Ni and the amorphous $Ni_{75}B_{15}Si_{10}$ alloy.

the single-crystalline Ni, the rms roughness significantly increased in an initial stage up to an ion dose of 8.92×10^{16} ions/cm^2 as well as the amorphous solid, subsequently, it continued to increase with ion dose, though the rate of increase in rms roughness in the ion dose range more than 8.92×10^{16} ions/cm^2 was lower than that less than 8.92×10^{16} ions/cm^2. As shown in Fig. 2, it appeared from SEM observation that very smooth machining was attained by FIB process for both the single-crystalline solid and the amorphous solid. However, the AFM observation revealed that there was difference in both surface topography and roughness from the nanometer-scopic view between the single-crystalline solid and the amorphous solid. This is likely to be related to the nature of smoothening process.

Surface evolution during FIB machining results from competition of roughening process and smoothening process. Roughening process is attributed to crystallographic factors, difference of local ion incident angle and non-uniform sputtering.[10] In this work, crystallographic factors are negligible because there are no grain boundaries, internal defects, other phases different from the matrix phase and differences in crystal orientation of each grain in single crystalline Ni and $Ni_{75}B_{15}Si_{10}$ alloy. It can be seen from Fig. 2 that the depth of hexagon holes is the same, *i.e.*, the sputtering rates for both materials are almost the same, so the difference of local ion incident angle is also negligible. Besides, non-uniform sputtering is concerned, difference of both the materials is the same due to the same FIB machining condition. On the other hand, smoothing is driven for reduction of the surface free energy and the main mechanisms are surface diffusion and viscous flow.[11,12] The spectrum of spatial frequencies contained in the surface structure may be given by[12,13]

$$\frac{d|h|^2}{dt} = -(Fq + Dq^4)h^2 \quad (1)$$

where h is the spectrum of spatial frequencies contained in the surface structure, t is time, F is γ/η (γ: the surface free energy, η: the viscosity), D is $2D_s\gamma\Omega^2\nu/kT$ (D_s: the surface diffusivity and Ω: the atomic volume, ν: the number of atoms per unit area of surface, k: the Boltzmann's constant, T: the absolute temperature) and q is the surface wave vector. Fq is representative of the smoothening rate by viscous flow and Dq^4 is representative of the smoothening rate by surface diffusion. Due to the different dependence of the smoothening rate on the magnitude of the surface wave vector between surface diffusion and viscous flow, short-range fluctuation decays more effective by surface diffusion and viscous flow makes long-range fluctuation decay effectively.[11] As shown in Fig. 4, the rms roughness of the single-crystalline Ni was smaller than that of the amorphous $Ni_{75}B_{15}Si_{10}$ alloy in the ion dose range less than 1.8×10^{18} ions/cm^2, however, the former was larger than the latter in the ion dose range more than 1.8×10^{18} ions/cm^2. Therefore, it is suggested that when the ion dose is low, surface diffusion plays an important role in smoothening during FIB machining because short-range fluctuation decays more effective by surface diffusion, while, when the ion dose is large, viscous flow effectively contributes to smoothening during FIB machining because long-range fluctuation decays more effectively by viscous flow.

4. Conclusion

The present work showed that surface evolution after FIB machining (30 keV and 187 pA) at doses of 8.92×10^{16}–2.68×10^{18} ions/cm^2 on a single-crystalline Ni and an amorphous $Ni_{75}B_{15}Si_{10}$ alloy have been investigated by AFM. The rms roughness increased with increasing ion dose and the transition of surface morphology from dot structure to ripple structure occurred during FIB machining in the single-crystalline Ni. On the other hand, the amorphous $Ni_{75}B_{15}Si_{10}$ alloy showed no such transition of surface morphology and held the rms roughness almost constant in an ion dose range more than about 1×10^{17} ions/cm^2. Therefore, it is suggested that surface diffusion, which is the primary smoothing mechanism for crystalline surfaces, plays an important role in smoothening during FIB machining when the ion dose is low, while viscous flow, which is dominant for amorphous surfaces, contributes to smoothening when the ion dose is large.

Acknowledgement

This work was supported by "Integrated Development of Materials and Processing Technology for High Precision Components" by the New Energy and Industrial Technology Development Organization.

REFERENCES

1) Y. Q. Fu, N. K. A. Bryan, O. N. Shing and H. N. P. Wyan: Sens. Actuators **79** (2000) 230–234.
2) R. Nassar, M. Vasile and W. Zhang: J. Vac. Sci. Technol. B **16** (1998) 109–115.
3) A. Lugstein, B. Basnar and E. Bertagnolli: J. Vac. Sci. Technol. B **20** (2002) 2238–2242.
4) Y. Ando and J. Ino: Wear **216** (1998) 115–122.
5) P. Sigmund: Phys. Rev. **184** (1969) 383–416.
6) H. Hosokawa, K. Shimojima, Y. Chino, Y. Yamada, C. E. Wen and M. Mabuchi: Mater. Sci. Eng. A **344** (2002) 365–367.
7) H. Hosokawa, K. Shimojima and M. Mabuchi: Philos. Mag. Lett. **84** (2004) 149–155.
8) N. S. Ong, Y. H. Koh and Y. Q. Fu: Microelectron. Eng. **60** (2002) 365–379.
9) H. Hosokawa, K. Shimojima, Y. Chino, Y. Yamada, C. E. Wen and M. Mabuchi: J. Mater. Sci. Lett. **21** (2002) 837–839.
10) R. M. Bradley and J. M. E. Harper: J. Vac. Sci. Technol. A **6** (1988) 2390–2395.
11) E. Chason, T. M. Mayer, B. K. Kellerman, D. T. McIlroy and A. J. Howard: Phys. Rev. Lett. **72** (1994) 3040–3043.
12) C. Herring: J. Appl. Phys. **21** (1950) 301–303.
13) W. W. Mullins: J. Appl. Phys. **30** (1959) 77–83.